# Entropic Lattice Boltzmann Study of Hydrodynamics in a Microcavity

By C. E. Frouzakis<sup>1</sup>, S. Ansumali<sup>1</sup>, I. V. Karlin<sup>1</sup>, and I. G. Kevrekidis<sup>2</sup>

<sup>1</sup>Aerothermochemistry and Combustion Systems Laboratory, Swiss Federal Institute of Technology Zurich (ETHZ), 8092 Zürich, Switzlerland

<sup>2</sup>Department of Chemical Engineering, Princeton University, NJ 08544-5263, USA

(Received 6 December 2004)

In flows through microdevices the continuum fluid mechanics description often breaks down and higher order corrections to the Navier–Stokes description arise both at the boundaries and in the bulk. The interaction between the flow geometry, rarefaction and compressibility is not completely understood for such flows. Recent advances in computational kinetic theory, such as the entropic lattice Boltzmann method, provide a simple and realistic framework which enable the systematic study of such interactions.

We consider a specific example of entropic lattice Boltzmann model and compare it with Grad's moment system. We show that for the model under consideration, the dispersion relation is closely related to that of Grad's ten-moment system. We perform a parametric study of the flow in a microcavity, which is a prototype problem, where the deviations from incompressible hydrodynamics can be studied conveniently. Simulation results obtained with the entropic lattice Boltzmann method are compared with those of the Direct Simulation Monte-Carlo method. Based on the parametric study, we discuss aspects of the interaction between rarefaction and compressibility.

## 1. Introduction

Flow in microdevices is an emerging application field for the fluid dynamics (Ho & Tai 1998; Beskok & Karniadakis 2001). Despite impressive experimental progress, understanding of the fluid mechanics in such devices is still incomplete. Microflows are highly subsonic but the continuum description of incompressible hydrodynamics often breaks down and higher order corrections to the Navier–Stokes description arise both at the boundaries and in the bulk. In principle, such flows can be studied using molecular level methods, such as the Direct Simulation Monte Carlo (DSMC) method (Bird 1994). However, these methods have severe limitations for subsonic flows. The number of particles required for geometries with large aspect ratios and the number of time steps required to reach the statistical steady state (the time step of DSMC is comparable to the collision time scale  $\sim 10^{-10} {\rm s}$ ), are prohibitively high for realistic simulations (Oran et al. 1998). Thus, an important focus of microflow research is to develop minimal and reliable computational models. Minimal kinetic models for microflows should have the following properties:

 $\bullet$  Parameter-free description of the slip-flow regime: For a dilute gas, the Knudsen number (the ratio of the mean free path to the characteristic length) in microdevices ranges from Kn  $\sim 0.001$  to Kn  $\sim 10$ , with most of the applications in the range of

Kn < 1. In this regime, continuum models like the Navier-Stokes equations with noslip boundary conditions are not valid. However, we know for example that the diffusive boundary condition at the molecular level (Cercignani 1975), provides a parameter free description of such flows (to describe rough surfaces more advanced boundary conditions might be needed, as for example see Cercignani & Lampis (1970)). The kinetic model should not introduce new parameters as compared to a complete molecular description. The slip velocity and analytical flow profiles for specific flow situations, known from the asymptotic theory of the Boltzmann equation, can be used to validate the boundary conditions in kinetic models of microflows.

• Correct description of non-hydrodynamic effects: Due to the subsonic nature of the flow, Grad's moment system in its linearized form becomes a good approximation for the slow flows (Ma  $\ll$  1, Re  $\sim$  1) (Grad 1958). The behavior of hydrodynamic and non-hydrodynamic modes for the Grad's moment system is well understood (Gorban & Karlin 2004). We are interested in kinetic models, which exhibit similar features. It should be noted, however, that Grad's systems are inconvenient as a numerical tool, mainly because of the ambiguity in the boundary conditions.

It has been shown by several groups that the entropic lattice Boltzmann model recovers the slip flow regime correctly in simple flow geometries (Ansumali & Karlin 2002b; Niu et al. 2003; Succi & Sbragaglia 2004; Ansumali et al. 2004). In order to understand the domain of validity of the method and its relationship to the Boltzmann equation, it is important to compare the model with Grad's system.

In the present work, we will consider a two dimensional entropic lattice model with nine discrete velocities (so-called D2Q9 lattice (Qian et al. 1992)). A parametric study of the lid-driven cavity flow is performed in order to understand the interaction of compressibility, rarefaction and boundary conditions. A spectral analysis of the flow at the steady state is performed to represent the dynamics of the moments in terms of the slow eigenfunctions. Such an analysis is a first step towards coarse-grained multi-scale system level simulation for microdevices (see for example Theodoropoulos et al. (2004); Kevrekidis et al. (2003)).

The work is organized as follows: In section 2, the discrete velocity model is presented. In section 3, the dispersion relation for the present model is compared with that of Grad's 10-moment system. In section 4, a brief review of the entropic lattice Boltzmann method is given. In section 5, a parameteric study of the flow in a microcavity is presented. In section 6, the stability analysis of the flow in a microcavity is presented.

### 2. Minimal Kinetic Model on D2Q9 Lattice

For the present model, the set of discrete velocities is:

$$c_x = \{0, 1, 0, -1, 0, 1-1, -1, 1\}, \quad c_y = \{0, 0, 1, 0, -1, 1, 1, -1, -1\}.$$
 (2.1)

The kinetic equation for the population,  $f_i \equiv f(x, \mathbf{c}_i, t)$ , as a function of the discrete velocity  $\mathbf{c}_i$ , position  $\mathbf{x}$  and time t, is written as (with Bhatnagar-Gross-Krook collision model):

$$\partial_t f_i + \mathbf{c}_i \cdot \partial_{\mathbf{x}} f_i = -\frac{1}{\tau} \left( f_i - f_i^{\text{eq}}(f) \right).$$
 (2.2)

The right hand side of this equation represents collisional relaxation to the local equilibrium,  $f_i^{\text{eq}}$ , on a time scale  $\tau$ . The local equilibrium distribution  $f_i^{\text{eq}}$  is the minimizer of

the discrete H function (Karlin et al. 1999; Ansumali et al. 2003):

$$H = \sum_{i=1}^{9} f_i \ln \left( \frac{f_i}{W_i} \right), \text{ with weights } W = \left\{ \frac{16}{36}, \frac{4}{36}, \frac{4}{36}, \frac{4}{36}, \frac{4}{36}, \frac{1}{36}, \frac{1}{36}, \frac{1}{36}, \frac{1}{36} \right\}. (2.3)$$

under the constraints of the local hydrodynamic fields:

$$\sum_{i=1}^{9} f_i^{\text{eq}}(f)\{1, c_{xi}, c_{yi}\} = \{\rho, j_x, j_y\},$$
(2.4)

where  $\rho$  is the local mass density, and  $j_{\alpha}$  is the local momentum density of the model. (It need to be reminded that the mass and the momentum densities of this model is not the mass and momentum densities of a real fluid. We need to establish the connection between the physically measurable densities and the densities appearing in the present model. This will be done in the next section, where the model will be compared to the Grad's system.) The explicit expression for  $f_i^{\text{eq}}$  is (Ansumali et al. 2003):

$$f_i^{\text{eq}} = \rho W_i \left( 2 - \sqrt{1 + 3u_x^2} \right) \left( 2 - \sqrt{1 + 3u_y^2} \right) \left( \frac{2u_x + \sqrt{1 + 3u_x^2}}{1 - u_x} \right)^{c_{xi}} \left( \frac{2u_y + \sqrt{1 + 3u_y^2}}{1 - u_y} \right)^{c_{yi}}, \tag{2.5}$$

where  $u_{\alpha} = j_{\alpha}/\rho$ , and the speed of the sound is  $c_s = 1/\sqrt{3}$ . In the hydrodynamic regime, the model recovers the Navier-Stokes equation with the viscosity coefficient  $\mu = p\tau$ , where  $p = \rho c_s^2$  is the pressure. For the boundary condition at the wall, a discrete form of the diffusive boundary condition for the Boltzmann equation is used (Ansumali & Karlin 2002b).

### 3. Grad's 10-moment System and the Minimal Kinetic Model

In this section, we consider the simple case of one-dimensional flow, and compare the dispersion relation with that of the linearized Grad's 10-moment system (because of the absence of the energy conservation, it is more appropriate to compare the present model with the 10-moment system, rather than with the 13-moment system).

## 3.1. The Linearized Moment System

It proves useful to represent the discrete velocity model as a moment system. For simplicity, we will consider the linearized version of the model. In the present model, linearization is required only for the collision term, this is at variance with Grad's moment systems where the advection term is also nonlinear. We choose the following nine moments (in non-dimensional form) as independent variables:

$$\mathbf{M} = \left\{ \frac{\gamma \rho}{\rho_0}, \frac{\sqrt{\gamma} j_x}{\rho_0 c_s}, \frac{\sqrt{\gamma} j_y}{\rho_0 c_s}, \frac{\gamma P}{\rho_0 c_s^2}, \frac{\gamma N}{\rho_0 c_s^2}, \frac{\gamma P_{xy}}{\rho_0 c_s^2}, \frac{\gamma^{3/2} q_x}{2\rho_0 c_s^3}, \frac{\gamma^{3/2} q_y}{2\rho_0 c_s^3}, \frac{\gamma^2 \psi}{2\rho_0 c_s^4} \right\}, \tag{3.1}$$

where

$$\psi = R_{yyyy} + R_{xxxx} - 2R_{xxyy} \tag{3.2}$$

is a scalar obtained from  $4^{th}$ -order moments  $(R_{\alpha\beta\gamma\theta} = \sum_{i=1}^{9} f_i c_{\alpha i} c_{\beta i} c_{\gamma i} c_{\theta i})$ , quantity  $N = \sum_{i=1}^{9} f_i (c_{xi}^2 - c_{yi}^2)/2 \equiv (P_{xx} - P_{yy})/2$  is the difference of the normal stresses, and  $q_{\alpha} = \sum_{i=1}^{9} f_i c_{\alpha i} c_i^2$  is the contraction of the third order moment  $Q_{\alpha\beta\gamma} = \sum_{i=1}^{9} f_i c_{\alpha i} c_{\beta i} c_{\gamma i}$ . The choice of a particular set of moments to represent the dynamics is arbitrary and is immaterial as long as set of linearly independent moments are chosen. Current choice

of moment is motivated from the Grad's 13- moment system. Time and space are made non-dimensional in such a way that for a fixed system size they can be measured in the units of mean free time and mean free length, respectively:  $\mathbf{x}' = \mathbf{x}/(L\mathrm{Kn}), t' = t/\tau$ , where  $\mathrm{Kn} = \tau c_s/(\sqrt{\gamma}L)$ . The linearized equations for these non-dimensional moments (from now on we use the the same notation for the non-dimensional variables) read:

$$\partial_{t}\rho + \gamma \,\partial_{x}j_{x} + \gamma \,\partial_{y}j_{y} = 0,$$

$$\partial_{t}j_{x} + \partial_{x}\left(P + N\right) + \partial_{y}P_{xy} = 0,$$

$$\partial_{t}j_{y} + \partial_{x}P_{xy} + \partial_{y}\left(P - N\right) = 0,$$

$$\partial_{t}P + \partial_{x}q_{x} + \partial_{y}q_{y} = (\rho - P),$$

$$\partial_{t}N + \partial_{x}\left(q_{x} - Q_{xyy}\right) - \partial_{y}\left(q_{y} - Q_{yxx}\right) = -N,$$

$$\partial_{t}P_{xy} + \partial_{x}Q_{yxx} + \partial_{y}Q_{yyx} = -P_{xy},$$

$$\partial_{t}q_{x} + \partial_{x}R_{xx\alpha\alpha} + \partial_{y}R_{xy\alpha\alpha} = (2\gamma j_{x} - q_{x}),$$

$$\partial_{t}q_{y} + \partial_{x}R_{xy\alpha\alpha} + \partial_{y}R_{yy\alpha\alpha} = (2\gamma j_{y} - q_{y}),$$

$$\partial_{t}\psi + \partial_{x}\left(\gamma^{2}j_{x} - \gamma q_{x}\right) + \partial_{y}\left(\gamma^{2}j_{y} - \gamma q_{y}\right) = (2\rho\gamma - \psi).$$

$$(3.3)$$

Furthermore, the lattice construction implies the following relations:

$$Q_{xyy} = 2q_x - 3\gamma j_x, \quad Q_{yxx} = 2q_y - 3\gamma j_y, \quad (3.4)$$

$$R_{xy\alpha\alpha} = 3\gamma P_{xy}, \quad R_{xx\alpha\alpha} = 3\gamma \left(P + \frac{1}{2}N\right) - \frac{1}{2}\psi, \quad R_{yy\alpha\alpha} = 3\gamma \left(P - \frac{1}{2}N\right) - \frac{1}{2}\psi. \quad (3.5)$$

Apart from the lack of conservation of the energy and linearity of advection, the model is similar to Grad's 13-moment system. However, in the present case a particular component of the  $4^{th}$ -order moment is also included as a variable. In other words, Grad's non-linear closure for the  $4^{th}$ -order moment is replaced by an evolution equation with a linear advection term. We note here that while the formulation of boundary conditions for Grad's moment system remains an open problem, the boundary conditions for the extended moment system (system 3.3,3.4, and 3.5) are well established (Ansumali & Karlin 2002b). One may conjecture that the fourth-order moment closure will deviate from Grad's closure only near the boundary. We also note that like any other Grad's system the present model reproduces the Navier-Stokes equation in the hydrodynamic limit (Karlin et al. 1999; Ansumali et al. 2003).

The moment system written in the present form also reveal the meaning of the densities appearing in model. The present moment system indicate that the dimensionless density of the moment system is dimensionless pressure of the real fluid in the low Mach number limit. Further, the momentum density should be identified with velocity in this limit of incompressible fluid. With this identification of the variables, we will compare the present moment system with Grad's system.

#### 3.2. One dimensional Grad's 10-moment system

For one-dimensional flows, Grad's 10-moment system (in non-dimensional form) can be written as (Gorban & Karlin 2004):

$$\partial_t p + \gamma \partial_x u_x = 0, \quad \partial_t u_x + \partial_x P_{xx} = 0, \quad \partial_t P_{xx} + 3\partial_x u_x = -(P_{xx} - p),$$
 (3.6)

where  $\gamma$  is the ratio of the specific heats of the fluid, and  $\gamma = (D+2)/D$  for a D-dimensional dilute gas. This model can be described in terms of its dispersion relation, which upon substitution of the solution in the form  $\sim \exp(\omega t + ikx)$  reads:

$$\omega^3 + \omega^2 + 3k^2\omega + \gamma k^2 = 0. {(3.7)}$$

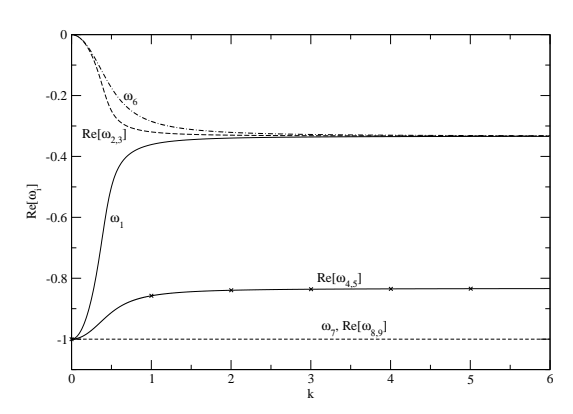


FIGURE 1. Real part of the solutions of the dispersion relation (equation (3.9)). Roots  $\omega_{2,3}$  and  $\omega_1$  correspond to Grad's subsystem (equation (3.6)). The real-valued root  $\omega_6$  and the complex conjugate roots  $\omega_{2,3}$  are extended hydrodynamic modes.

Eq. 3.7 provides the simplest instance of the invariance condition which can be used to study the effectiveness of different approximations to construct invariant manifolds (see for details Gorban & Karlin (2004); Karlin & Gorban (2002)). As the time and space are measured in the unit of mean-free time and length respectively, the low wave-number asymptotic represents the dynamics happening at large scale (continuum scale of Kn  $\ll$  1), while the high-wave number limit represent the molecular scales quantified by Kn  $\gg$  1. The low wave-number (Kn  $\ll$  1) asymptotic,  $\omega_l$ , and the large wave-number (Kn  $\gg$  1) asymptotic,  $\omega_h$ , are:

$$\omega_{l} = \left\{ \frac{(-3+\gamma)}{2} k^{2} \pm i\sqrt{\gamma}k, -1 - (-3+\gamma)k^{2} \right\}, \quad \omega_{h} = \left\{ \frac{(-3+\gamma)}{6} \pm i\sqrt{3}k, -\frac{\gamma}{3} \right\}.$$
(3.8)

The two complex conjugated modes (acoustic modes) of the  $O(k^2)$  dynamics, are given by first two roots of  $\omega_1$ , and represent the continuum hydrodynamics limit (Navier-Stokes approximation) of the model. The third root in this limit is real and negative, which shows the relaxational behavior of the non-hydrodynamic variable (stress), in particular dominant contribution -1 is rate of relaxation towards equilibrium value, while the next correction depict the slaving of viscous forces, which amounts to the constitutive relation for stress  $((-3+\gamma)/2k^2)$ . Further more, the  $k^2$  dependence of the relaxation term justifies the assumption of scale-separation (higher the wave-number, faster is the relaxation). The real part of high wave-number solution  $\omega_h$  is independent of k, which shows that the relaxation at very high Knudsen number (Knudsen gas limit) is same for all wavenumber. Thus, the assumption of scale-separation is not valid for high Knudsen number dynamics.

### 3.3. Dispersion Relation for Model Moment System

The dispersion relation for the one-dimensional version of the moment system (3.3) (i.e. neglecting all derivatives in the y-direction) is:

$$(\omega^3 + \omega^2 3k^2 + \omega + k^2)(\omega^3 + 2\omega^2 + (3k^2 + 1)\omega + k^2)(1 + \omega)((1 + \omega^2) + 2k^2) = 0.$$
 (3.9)

The real parts of the solutions of this polynomial equation (attenuation rates) are plotted in Figure 3.3.

It is clear that for one-dimensional flows, the dynamics of three of the moments are decoupled from the rest and follow those of the one dimensional Grad's 10-moment

system. The coupling of the six higher order moments with the first three moments is unidirectional. As a consistency check, the eigen-spectrum of the collision is recovered at k=0, i.e., three of the modes relax with  $\omega=0$ , while the other six relaxes with  $\omega=-1$ . We remind that the three modes with  $\omega=0$  at k=0 are hydrodynamic modes, while the other six modes are kinetic modes.

The similarity between Grad's approximation and the present model is an important fingerprint of the relaxational or kinetic nature of the model. It should be remarked here, that in the case of two-dimensional flows, the agreement between the present model and Grad's system is only qualitative. The present moment system is isotropic only up to  $O(k^2)$ . Thus, the dispersion relation of the model on D2Q9 lattice is expected to match the one of Grad's system only up to the same order. In the hydrodynamic and slip-flow regime, this isotropy is sufficient, while in the transition-flow regime more detailed entropic lattice Boltzmann models like the model on D2Q16 lattice should be used (Ansumali et al. 2003).

In the presence of boundaries or non-linearity, it is more convenient to use numerical simulation. Before highlighting the simulation results, we briefly describe the entropic lattice Boltzmann model.

#### 4. The Entropic Lattice Boltzmann Discretization

The time stepping in this discretization scheme is performed through an over-relaxation collisional process and linear convection. The monotonicity constraint on the H function is imposed through the following procedure: In the first step, populations are changed in the direction of the collision in such a way that the H function remains constant (Karlin et al. 1999; Boghosian et al. 2001). In the second step, dissipation is introduced and the magnitude of the H function decreases. Thus,

$$f_i(\mathbf{x}, \delta t) = f_i(\mathbf{x} - \mathbf{c}_i \delta t, 0) + \alpha \beta \left[ f_i^{\text{eq}}(\mathbf{x} - \mathbf{c}_i \delta t, 0) - f_i(\mathbf{x} - \mathbf{c}_i \delta t, 0) \right], \tag{4.1}$$

were  $\beta$  is the discrete form of the relaxation frequency related to  $\tau$ , and  $\alpha$  is obtained by solving a non-linear equation, which is derived from the discrete-time H-theorem:

$$\beta = \frac{\delta t}{2\tau + \delta t}, \quad H(\mathbf{f}) = H((1 - \alpha)\mathbf{f} + \alpha\mathbf{f}^{eq}). \tag{4.2}$$

Close to local equilibrium,  $\alpha$  is equal to 2. The local adjustments of the relaxation time (via the parameter  $\alpha$ ), as dictated by compliance with the H theorem, guarantee positivity of the distribution function also for the case of discrete time steps, thereby ensuring the non-linear stability of the numerical scheme.

# 5. Flow in a driven microcavity

The two-dimensional flow in a lid-driven cavity is simulated with ELBM over a range of Knudsen numbers defined as Kn = Ma/Re. In the simulations, the Mach number is fixed at Ma = 0.01 and the Reynolds number, Re is varied. Here, we present results for Kn=0.001, 0.01, and 0.1. Initially, the fluid in the cavity is at rest and the upper wall of the domain is impulsively set to motion with  $u_{\rm lid} = c_s * {\rm Ma} = \sqrt{3} * {\rm Ma}$ . The diffusive boundary conditions are imposed at the walls (Ansumali & Karlin 2002b), and the domain was discretized using 151 points in each spatial direction. Time integration is continued till the steady state is established. A typical simulation time for 50,000 time steps on a Pentium 4 2.4 GHz is around 3 hr.

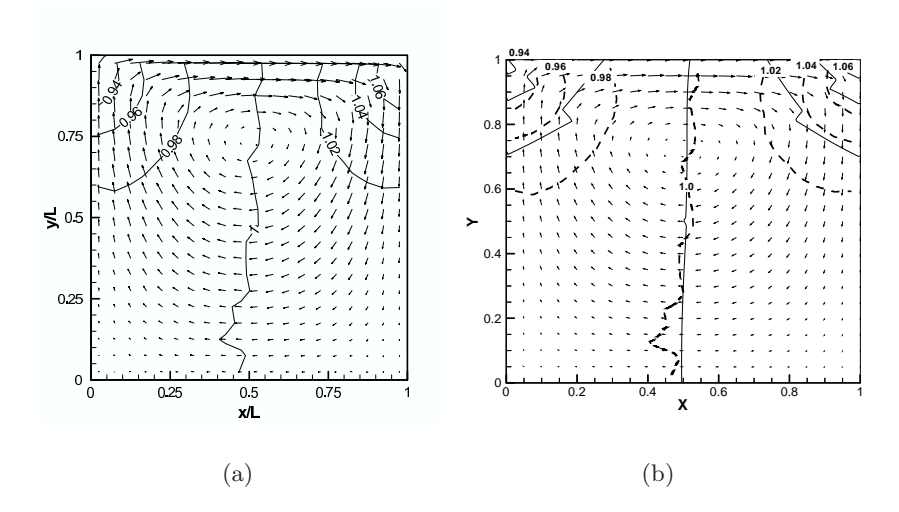


FIGURE 2. Flow in a micro-cavity for Kn=0.1 and Ma=0.14: (a) DSMC simulation (Jiang *et al.* 2003), (b) velocity vector plot and density isolines from ELBM (solid lines) with the DSMC density isolines (dashed lines) superimposed.

## 5.1. Validation with DSMC simulation of microcavity

As the present model does not conserve energy, it is expected to give physically relevant results only when the isothermal assumption is justified. This restricts the domain of validity to the hydrodynamic and the slip-flow regimes (but it still covers a wide domain of fluid dynamics for continuum hydrodynamics and microflows). In the hydrodynamic regime, the model was validated using results available from continuum simulations (Ansumali & Karlin 2002a). For higher  $\mathrm{Kn} \sim 0.01$ , we compared our results with the DSMC simulation of (Jiang et al. 2003). The good agreement between the DSMC simulation and the ELBM results can be seen in figure 2. It can be concluded, that even for finite Knudsen number, the present model provides semi-quantitative agreement, as far as flow profile is concerned. We remind here again, that the dimensionless density in the present model is dimensionless pressure of a real fluid, so for quantitative comparision, the density of ELBM model should be compared with the pressure computed from DSMC.

#### 5.2. A parametric study of flow in a microcavity

Figure 3 shows the dimensionless density profiles with the streamlines superimposed for  $\mathrm{Kn}=0.001,0.01,0.1$ . For  $\mathrm{Kn}=0.001$  (Re = 10), the behavior expected from continuum simulations with a large central vortex and two smaller recirculation zones close to the lower corners can be observed. As the Knudsen number is increased, the lower corner vortices shrink and eventually disappear. The superimposed streamlines show that the flow becomes simpler as Kn increases and the streamlines tend to align themselves with the walls. Contrary to the results of Nie et al. (Nie et al. 2002) obtained with bounce-back boundary conditions, we did not observe the movement of the center of the large vortex towards the lid with increasing Kn. This movement may be an artifact of the boundary conditions used.

The density profiles, as a function of Kn, demonstrate that the assumption of incompressibility is well justified only in the continuum regime, where the density is essentially constant away from the corners. This observation is consistent with the conjecture that

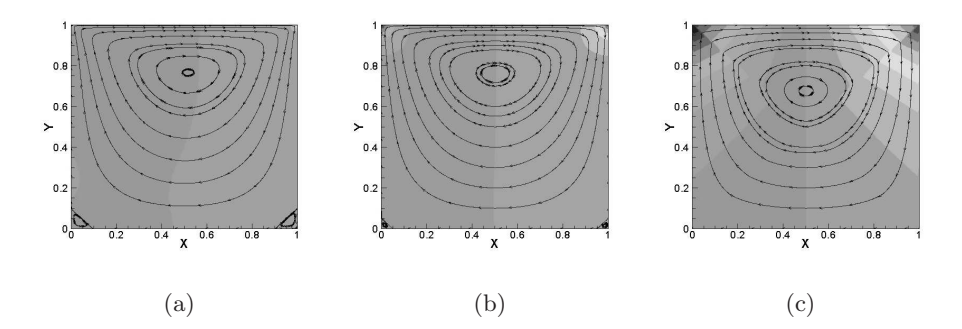


FIGURE 3. Density isocontours for (a) Kn=0.001, (b) Kn=0.01 , and (c) Kn=0.1 (0.995  $\leq \rho \leq$  1.005). Superimposed are the streamlines.

incompressibility requires smallness of Mach as well as Knudsen number. In hydrodynamic theory, the density waves decay exponentially fast (with the rate of relaxation proportional to Kn for a dilute gas) leading effectively to incompressibility. Thus, it is expected that the onset of incompressibility will be delayed as the Knudsen number increases, i.e. incompressibility is a feature of the Navier-Stokes limit of the kinetic equation. Further, as Kn increases, Re decreases and viscosity is not sufficient to smoothen out discontinuities in density and the discontinuity at the corners of the cavity spreads over the rest of the domain along the diagonals. These results clearly indicate that for finite Knudsen number flows, incorporation of correct thermohydrodynamics is necessary to obtain quantitatively correct results.

The maximum (dimensionless) x-velocity component of the fluid on the lid is 0.99, 0.9, and 0.35 for the three cases considered, a result of the increasing slip with Kn. Figure 4 compares the isocontours of  $\sigma_{xy} = -\tau c_s^2(\partial_y j_x + \partial_x j_y)$  (upper row) with  $P_{xy} - P_{xy}^{eq}$ , the non-equilibrium part of the corresponding moment (lower row). The differences observed for Re  $\leq 0.1$  result from deviations from the Navier-Stokes behavior. Away from the walls, the hydrodynamics is described well in terms of the first correction from equilibrium obtained from the Chapman-Enskog expansion.

Figure 5 shows a scatter plot of the xy component of the stress tensor  $(\sigma_{xy} = \mu(\partial v/\partial x + \partial u/\partial x))$  with the non-equilibrium part of the corresponding component of the moment vector  $\mathbf{M}$  for all points in the domain. The dashed straight line of slope equal to one corresponds to Navier-Stokes behavior. For low Kn, most points lie along this line. As Kn is increased, the behavior becomes non-hydrodynamic for more and more points, which are now located also in the bulk. For Kn=0.1, almost all points show non-hydrodynamic behavior. An indication of the location of the points is shown in figure  $\mathbf{5}(\mathbf{c})$ , where the lines starting at A-E connect points at equal y. The line starting from A corresponds to the points on the moving lid, while lines from B-E to points lying 1-4 y-isolines below the it  $(y_A=1.0, y_B=0.933, y_C=0.987, y_D=0.98, y_E=0.973)$ . The starting points A-E are located on the right wall.

#### 6. Stability analysis

The ELBM code was coupled with ARPACK (Lehoucq *et al.* 1998) to compute the leading eigenvalues and the corresponding eigenvectors of the Jacobian of the map defined by equation (4.1) at the computed steady states. In all cases, the eigenvalues are within

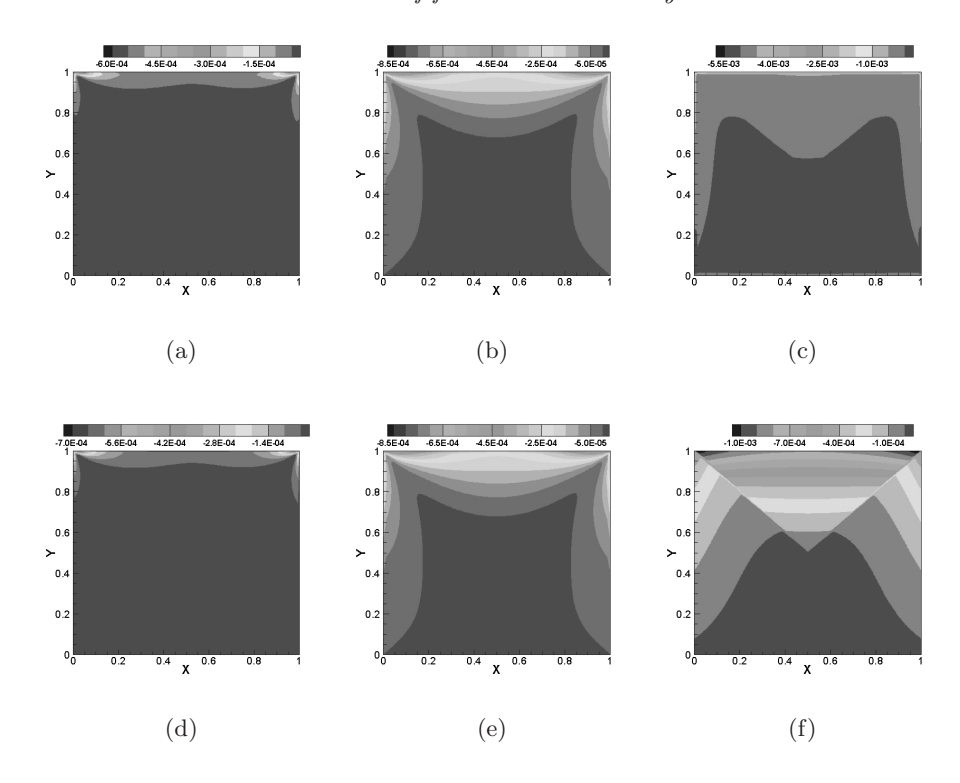


FIGURE 4. Stress component  $\sigma_{xy}$  (upper row) and  $P_{xy} - P_{xy}^{eq}$  (lower row) for Kn = 0.001 (a-d), Kn = 0.01 (b-e), and Kn = 0.1 (c-f), respectively.

the unit circle. The leading one is always equal to one (reflecting mass conservation), and the corresponding eigenvector captures most of the structure of the steady state.

Furthermore, in the hydrodynamic regime (Kn < 0.001), the accuracy of reconstruction of moments from the leading eigenvector is essentially independent of Knudsen number. This is in agreement with the understanding that in this regime molecular details (i,e, the rate of the decay of density wave in this limit of low Knudsen and low Mach flows) should not play any role. As the Knudsen number increases (Kn < 0.1), the accuracy of reconstruction decreases, suggesting that in the slip- and transitional-flow regime more and more eigendirections get excited. Adding a few more eigendirections does not reduce the difference between the moments computed directly and from the eigenfunction expansion. Our conjecture is that this happens because when the Knudsen number is small the incompressibility assumption is a good approximation, and can be captured by the leading eigendirections.

As Knudsen number decreases, eigenvalues tend to get clustered close to the unit circle (Figure 6), and more slowly decaying modes appear.

## 7. Conclusion

The entropic lattice Boltzmann model can be used as an efficient computational tool for the simulation of flow in microdevices. The dispersion relation of the one-dimensional model was compared with that of Grad's 10-moment system. The close relationship between the two models was highlighted, showing that Grad's moment approximation can be recovered as a special case. The model was used for the simulation of the flow in

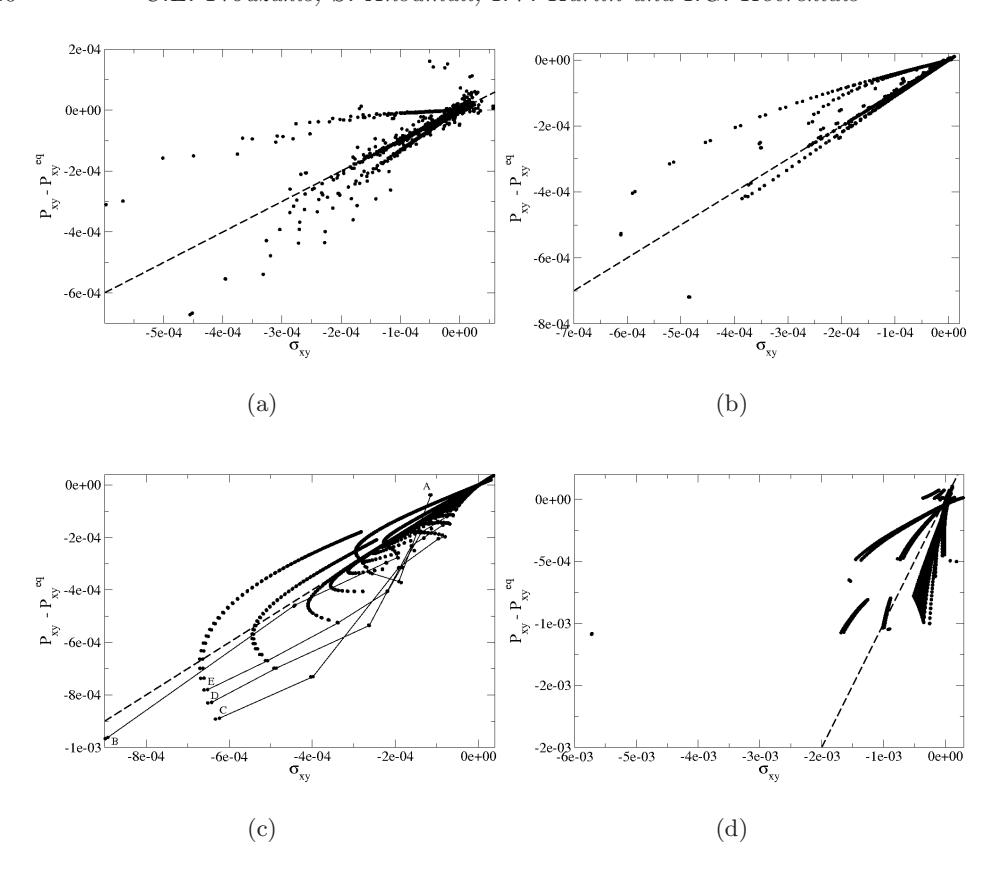


FIGURE 5. Deviation from hydrodynamic behavior (straight dashed line):  $P_{xy}-P_{xy}^{eq}$  plotted as a function of the stress component  $\sigma_{xy}$  for (a) Kn = 0.001, (b) Kn = 0.001, (c) Kn = 0.01 (see text for letters A-E) (d), Kn = 0.1

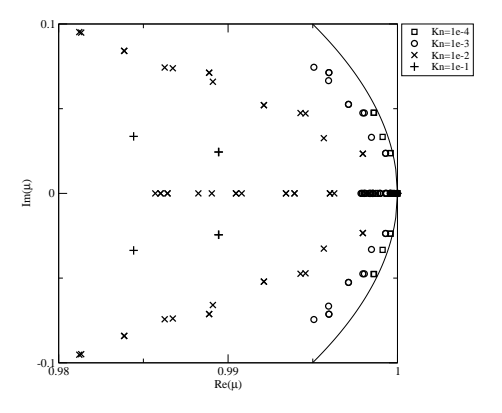


Figure 6. Leading eigenvalues of the map defined by equation (4.1)

a microcavity over a range of Knudsen numbers, showing good agreement with DSMC results from the literature. The available results show that the present model is capable of describing microflows in the slip-flow regime. Furthermore, the assumption of incompressibility is questionable for microflows. A more detailed analysis using the thermal entropic lattice Boltzmann model is a subject of future studies.

#### REFERENCES

- Ansumali, S. & Karlin, I. V. 2002a Entropy Function Approach to the Lattice Boltzmann Method. J. Stat. Phys. 107(1-2), 291–308.
- Ansumali, S. & Karlin, I. V. 2002b Kinetic Boundary Condition for the Lattice Boltzmann Method. Phys. Rev. E 66(2), 026311.
- Ansumali, S., Karlin, I. V. & Öttinger, H. C. 2003 Minimal Entropic Kinetic Models for Simulating Hydrodynamics. *Europhys. Lett.* **63(6)**, 798–804.
- Ansumali, S., Karlin, I. V. & Öttinger, H. C. 2004 Thermodynamic Theory of Incompressible Hydrodynamics .
- Beskok, A. & Karniadakis, G. E. 2001 Microflows: Fundamentals and Simulation. Springer, Berlin.
- Bird, G. A. 1994 Molecular Gas Dynamics and the Direct Simulation of Gas Flows. Theory and Application of the Boltzmann Equation. Oxford University Press.
- Boghosian, B. M., Yepez, J., Coveney, P. V. & Wagner, A. J. 2001 Entropic Lattice Boltzmann Methods. *Proc. Roy. Soc. Lond.* 457(2007), 717–766.
- CERCIGNANI, C. 1975 Theory and Application of the Boltzmann Equation. Scottish Academic Press, Edinburgh.
- CERCIGNANI, C. & LAMPIS, M. 1970 Find it out. Transport Theory statist. Phys. 1, 101.
- Gorban, A. N. & Karlin, I. V. 2004 Invariant Manifolds for Physical and Chemical Kinetics. Springer, Berlin Heidelberg.
- GRAD, H. 1958 Principles of the Kinetic Theory of Gases. Handbuch der Physik XII.
- Ho, C.-M. & Tai, Y.-C. 1998 Micro-Electro-Mechanical-Systems(MEMS) and Fluid Flows. *Annu Rev. Fluid Mech.* **30**, 579–612.
- JIANG, J.-Z., J., F. & SHEN, C. 2003 Statistical simulation of micro-cavity flows. 23rd Int. Symposium on Rarefied Gas Dynamics pp. 784-790.
- Karlin, I. V., Ferrante, A. & Öttinger, H. C. 1999 Perfect Entropy Functions of the Lattice Boltzmann Method. *Europhys. Lett.* 47, 182–188.
- KARLIN, I. V. & GORBAN, A. N. 2002 Hydrodynamics from Grad's Equations: What can We Learn from Exact Solutions? *Ann. Phys. (Leipzig)* 11, 783–833.
- Kevrekidis, I. G., Gear, C., Hyman, J. M., Kevrekidis, P. G., Runborg, O. & Theodor-opoulos, C. 2003 Equation-free, Coarse-grained Multiscale Computation: Enabling Microscopic Simulators to Perform System -level Analysis. *Comm. Math. Sci.* 1, 715–762.
- Lehoucq, R., Sorensen, D. & Yang, C. 1998 ARPACK Users' Guide: Solution of Large-Scale Eigenvalue Problems with Implicitly Restarted Arnoldi Methods. SIAM.
- NIE, X., DOOLEN, G. & SHEN, S. 2002 Lattice-Boltzmann simulations of fluids flows in MEMS. J. Stat. Phys. 107(1-2), 279–289.
- Niu, X. D., Shu, C. & Chew, Y. 2003 Lattice boltzmann BGK Model for Simulation of Micro Flows. Euro. Phys. Lett. 67, 600–606.
- ORAN, E. S., OH, C. K. & CYBYK, B. Z. 1998 Direct Simulation Monte Carlo: Recent Advances and Applications. *Annu Rev. Fluid Mech.* **30**, 403–441.
- QIAN, Y. H., D'HUMIERES, D. & LALLEMAND, P. 1992 Lattice BGK Models for Navier-Stokes Equation. *Europhys. Lett.* **17**, 479–484.
- Succi, S. & Sbragaglia, M. 2004 Analytical Calculation of Slip Flow in Lattice Boltzmann Models with Kinetic Boundary Conditions. http://arxiv.org/abs/nlin.CG/0410039.
- Theodoropoulos, C., Sankaranarayanan, K., Sundaresan, S. & Kevrekidis, I. G. 2004 Coarse Bifurcation Studies of Bubble Flow Lattice Boltzmann Simulations. *Chem. Eng. Sci.* **59**, 2357–2362.